Climate Risk Management 13 (2016) 31–42

Contents lists available at ScienceDirect

Climate Risk Management

journal homepage: www.elsevier.com/locate/crm

How will climate change affect the vegetation cycle over France? A generic modeling approach

Nabil Laanaia [a], Dominique Carrer [a], Jean-Christophe Calvet [a,*], Christian Pagé [b]

[a] CNRM, UMR3589 (Météo-France, CNRS), 42 Avenue Gaspard Coriolis, Toulouse, France
[b] CECI, CERFACS – CNRS, 42 Avenue Gaspard Coriolis, Toulouse, France

ARTICLE INFO

Article history:
Received 1 June 2015
Revised 7 April 2016
Accepted 14 June 2016
Available online 15 June 2016

Keywords:
Climate change
Adaptation
Modeling
Agriculture
Forestry
Phenology
Soil moisture

ABSTRACT

The implementation of adaptation strategies of agriculture and forestry to climate change is conditioned by the knowledge of the impacts of climate change on the vegetation cycle and of the associated uncertainties. Using the same generic Land Surface Model (LSM) to simulate the response of various vegetation types is more straightforward than using several specialized crop and forestry models, as model implementation differences are difficult to assess. The objective of this study is to investigate the potential of a LSM to address this issue. Using the SURFEX ("Surface Externalisée") modeling platform, we produced and analyzed 150-yr (1950–2100) simulations of the biomass of four vegetation types (rainfed straw cereals, rainfed grasslands, broadleaf and needleleaf forests) and of the soil water content associated to each of these vegetation types over France. Statistical methods were used to quantify the impact of climate change on simulated phenological dates. The duration of soil moisture stress periods increases everywhere in France, especially for grasslands with, on average, an increase of 9 days per year in near-future (NF) conditions and 36 days per year in distant-future (DF) conditions. For all the vegetation types, leaf onset and the annual maximum LAI occur earlier. For straw cereals in the Languedoc-Provence-Corsica area, NF leaf onset occurs 18 days earlier and 37 days earlier in DF conditions, on average. On the other hand, local discrepancies are simulated for the senescence period (e.g. earlier in western and southern France for broadleaf forests, slightly later in mountainous areas of eastern France) for both NF and DF. Changes in phenological dates are more uncertain in DF than in NF conditions in relation to differences in climate models, especially for forests. Finally, it is shown that while changes in leaf onset are mainly driven by air temperature, longer soil moisture stress periods trigger earlier leaf senescence over most of France. This shows that developing *in situ* soil moisture networks could help monitoring the long-term impacts of climate change.

1. Introduction

Adapting agriculture and forestry to climate change in a global context of rising demand for food and energy will be a key objective in the next decades. The basic information needed to build adaptation strategies is provided by impact models able to simulate vegetation growth in response to climate variables (Tubiello et al., 2007). The latter are provided by climate models. Both climate and impact models are affected by uncertainties, which have to be described and quantified as much as possible (e.g. Déqué and Somot, 2010; Soussana et al., 2010). In many European countries, agricultural and forestry practices

* Corresponding author.
E-mail address: jean-christophe.calvet@meteo.fr (J.-C. Calvet).

http://dx.doi.org/10.1016/j.crm.2016.06.001
2212-0963/

present local differences related to soil characteristics and, also, often related to local climates. Therefore, downscaling the large scale information given by global climate models is key. Moreover, an important component of adaptation is the development of new ground networks able to monitor biophysical indicators such as soil moisture (Calvet et al., 2007) and methods permitting the identification of vulnerable areas where the added value of such networks would be high.

In this study, we focus on metropolitan France, and we address local aspects of the impact of climate change on vegetation growth using the SURFEX (“Surface Externalisée”) modeling platform (Masson et al., 2013). The IPCC climate simulations, either CMIP3 A1B or CMIP5 RCP, show significant trends towards more precipitation in northern Europe and less precipitation in southern Europe and the Mediterranean basin (Jacob et al., 2014). From this point of view, France lies in an area between northern and southern Europe, where trends in precipitation are less pronounced. However, the marked increase in air temperature (T_{air}) may enhance evapotranspiration in spite of the antitranspirant action of CO_2 on plants. This may trigger a soil water deficit at springtime, earlier than under the present climate, and increase the irrigation demand (Calvet et al., 2008).

In order to simulate the impact of climate change on cultivated plant species, Brisson and Levrault (2010) used specific crop and forestry models over 12 sites representative of the main climatic regions in France. Their simulations suggested that wheat yields and the forage production could slightly increase in the future. On the other hand, the viability of forests, vineyards, and summer crops such as maize could be impacted by more frequent droughts in many regions. Loustau et al. (2005) used several forestry models over 5 locations in French plains. Their simulations indicated “a slight increase in potential forest yield until 2013–2050, followed by a plateau or a decline around 2070–2100”. These trends were more or less pronounced from one location to another and from one tree species to another.

As past studies have focused on a limited number of sites in France, there is a need for more extensive evaluation of the plant phenology response across species. Models able to represent various vegetation types have been developed in the last two decades. They rely on generic approaches permitting the simulation of land surface water, energy and CO_2 fluxes, together with soil moisture and vegetation biomass. In this study, we used the Interactions between Soil, Biosphere, and Atmosphere model (ISBA) developed by Meteo-France for meteorological, hydrological and climatic applications. The CO_2-responsive version of this model (Calvet and Soussana, 2001; Gibelin et al., 2008) is able to simulate plant growth and carbon storage. The model uses relatively few parameters while representing key processes. In particular, drought-avoiding and drought-tolerant plants can be distinguished thanks to a refined representation of the effects of soil water deficit on photosynthesis parameters (e.g. mesophyll conductance). Phenology is directly driven by photosynthesis and, using satellite leaf area index (LAI) products, Szczypta et al. (2014) showed that realistic LAI simulations can be obtained over Europe.

This work aims at assessing uncertainties of future trends on biophysical variables (leaf onset, leaf senescence, maximum LAI) for four vegetation types (rainfed straw cereals and grasslands, broadleaf forests, needleleaf forests) over a large number of sites representative of the agricultural and forest regions in France. Maize and vineyards are not considered as they are not explicitly represented in our simulations. As a key objective of this study is to quantify the impact of uncertainties in climate simulations, we use an ensemble of eleven climate models (Fig. 1) to drive the ISBA model. We apply classical statistical methods to assess: (1) trends in time series of downscaled simulations of biophysical variables and plant phenology indicators, (2) the consistency of the various climate simulations at a given location. Finally, the analysis of the spatial variability of the response of plant growth to climate change is investigated and the main spatial patterns identified in this study are summarized.

The climate simulations and the ISBA land surface model are presented in Section 2, together with the design of the simulations of biophysical variables. The results are shown in Section 3 and discussed in Section 4. The conclusions of this study are summed up in Section 5.

2. Material and methods

2.1. Climate simulations

The downscaled climate simulations used in this study are derived from the SCRATCH2010 database (http://www.cerfacs.fr/~page/scratch/), which has been used in various climate change impact studies in France (e.g. Gouache et al., 2012; Habets et al., 2013). SCRATCH2010 climate simulations are generated using a statistical downscaling method applied to global large-scale climate simulations. The methodology is described in Boé et al. (2006), and in Boé and Terray (2008). It is based on weather-typing and builds on the physical links between the large-scale circulation and the local scale climate, from which statistical relationships can be derived. The spatial scale of representation is changed but the temporal distribution of weather variables is close to the parent global simulation. This statistical downscaling method is used to produce climate projections at a fine scale over France (8 km by 8 km), at a hourly time step. It is first trained on a reference period using observations to define the statistical relationships, and then applied to the climate simulations. The reference atmospheric reanalysis used to train the method is “Système d’Analyse Fournissant des Renseignements A la Neige” (SAFRAN) (Durand et al., 1993; Quintana-Segui et al., 2008). SAFRAN provides hourly values of liquid and solid precipitation, incoming solar radiation, incoming longwave radiation, air temperature, air humidity, atmospheric pressure, and wind speed over France. Boé et al. (2006) showed that the climatology derived from the downscaled climate simulations for past decades is very close to the observed climatology. The original large scale climate simulations correspond to the CMIP3 Special Report on Emission

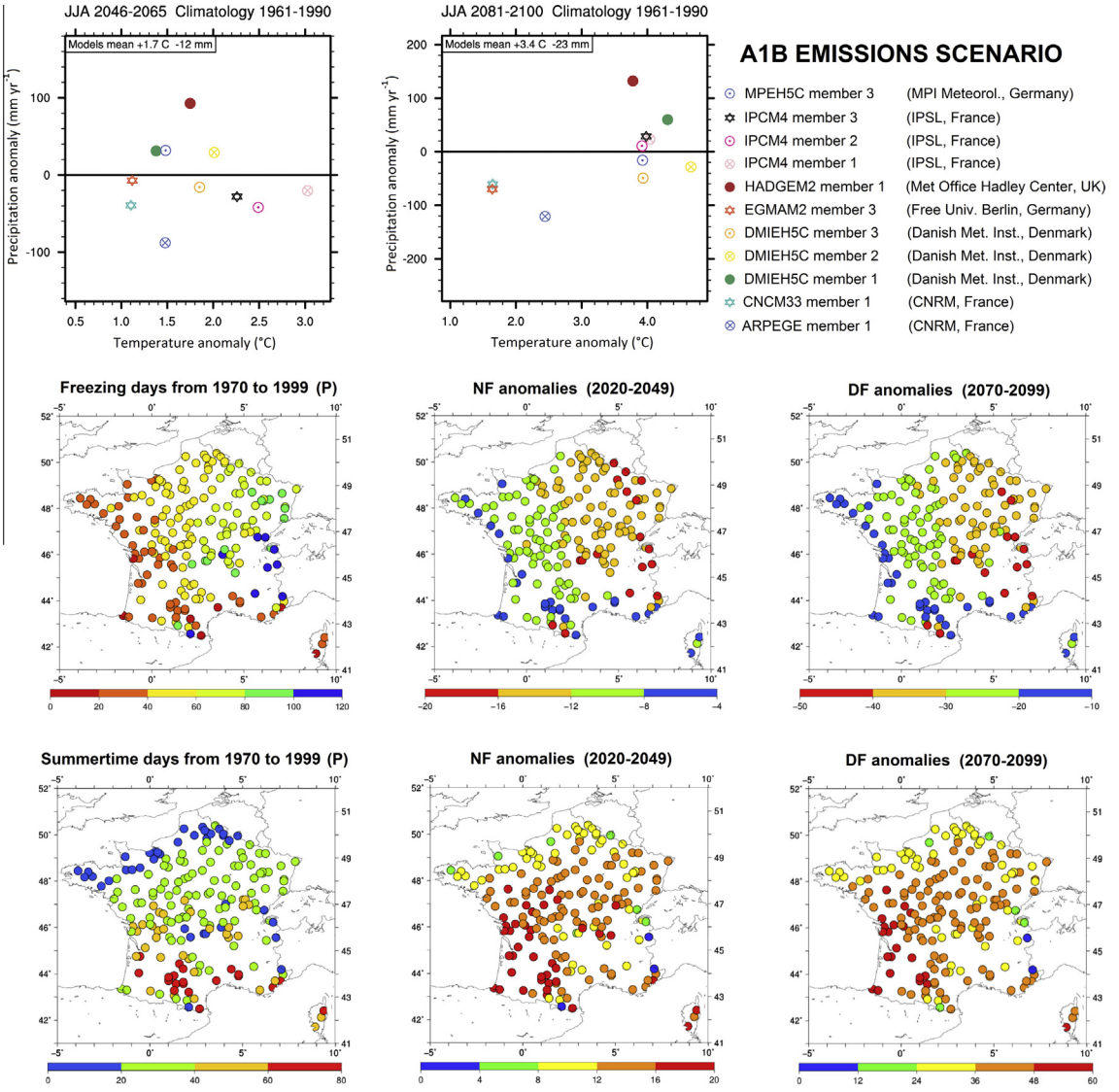

Fig. 1. The eleven downscaled A1B climate simulations used in this study. (Top, from left to right) average summertime (June–July–August) cumulated precipitation anomalies vs. air temperature anomalies for 2046–2065 and 2081–2100, with respect to the 1961–1990 period. (Middle, from left to right) average number of freezing days for the past ("P", from 1970 to 1999), and anomalies (in days) for near-future ("NF", from 2020 to 2049) and distant future ("DF", from 2070 to 2099). (Bottom, from left to right) average number of summertime days for P, and anomalies (in days) for NF and DF. Freezing and summertime days are defined as days with at least one hourly air temperature value below 0° and above 25°, respectively, at 191 locations.

Scenario (SRES) A1B scenario (IPCC, 2000). In order to produce an estimate of potential uncertainty through a broad sampling of future possibilities, sampling both chaotic variability and uncertainty in climate modeling (Harding et al., 2015), we used eleven climate simulations, listed in Fig. 1. They cover a 150-yr period, from 1950 to 2099. Three periods are considered: near future (NF) (2020–2049), distant future (DF) (2070–2099) and a reference past period P (1970–1999). The average cumulated precipitation and air temperature anomalies of the climate simulations over France are shown in Fig. 1 for summertime. At summertime, the sign of the precipitation anomaly varies from one climate simulation to another and the same results are found for the other seasons (not shown). This illustrates the difficulty to predict the precipitation anomalies for this part of Europe. More details about the downscaled climate simulations can be found in Pagé and Terray (2010) and Pagé et al. (2010). We used a single climatic scenario (A1B), which is restrictive. In future works, the use of other scenarios such as RCP (Jacob et al., 2014) will help characterize the uncertainties, especially in DF conditions.

2.2. Selection of representative sites

The downscaled climate model inputs are available on a regular grid of 8 km by 8 km, representing 8602 grid-cells. Since we took the option to use eleven climate models we conducted our study for a limited number of sites in France, due to

computational cost constrains. The ISBA simulations were made for a subset of 191 grid-cells representing the main French agricultural and forest regions. This subset of 191 grid-cells consists of the 45 cropland and 48 grassland homogeneous areas used in Calvet et al. (2012), of the 12 sites considered by Brisson and Levrault (2010), and of 86 forested areas (one in each eco-regions in France as defined by IFN, 2011). Fig. 1 shows the spatial distribution of the 191 sites.

2.3. The ISBA land surface model

In this study, we use these latest improvements of the model within the SURFEX version 7.3 software. This version of the model is similar to the one validated using satellite LAI products by Lafont et al. (2012) and Szczypta et al. (2014), except for the addition of a subroot-zone soil layer (Boone et al., 1999) and an enhanced multilayer canopy radiative transfer model (Carrer et al., 2013). The values of the ten key parameters of the model are listed in Table 1 for the vegetation types considered in our simulations. Key parameters of the photosynthesis model respond to the soil water stress permitting the representation of drought-avoiding and drought-tolerant responses to drought. For low vegetation and for trees, the response to drought is based on the meta-analysis of Calvet (2000) and Calvet et al. (2004), respectively. The intrinsic leaf-level water use efficiency (WUE) depends on the photosynthesis parameters and on [CO_2]. WUE responds to soil moisture: in the drought-avoiding (-tolerant) approach, WUE increases (decreases) in response to drought, provided the fraction of the extractable soil moisture content fraction is higher than a critical Soil Wetness Index value (SWI_C).

The surface water, energy, and CO_2 fluxes are computed separately for all the vegetation types together with separate soil water storage. Different soil water storage capacities are used to differentiate forests from low vegetation, in relation to contrasting rooting depths. The root-zone depth and the soil depth values for low vegetation are 1.5 m and 2.0 m, 2.0 m and 3.0 m for high vegetation, respectively. Relatively low uniform values of root-zone soil water holding capacity are obtained: 129 mm for low vegetation and 172 mm for high vegetation, on average. However, additional water can be used by the plants through capillary rises from base-flow soil layers. The water budget is calculated, which allows the simulation of the surface and of the root zone moisture. The latter is used to characterize the soil water stress.

The ISBA model was extensively validated and compared to a large variety of observations such as surfaces fluxes (Carrer et al., 2012; Balzarolo et al., 2014; Garrigues et al., 2015), and satellite-derived LAI and soil moisture (Lafont et al., 2012; Szczypta et al., 2014). In order to make sure that the ISBA model captures known phenomena, the meta-analysis of Yin (2002), based on 170 data cases of 62 species compiled from the literature, is used to ensure credibility for future estimates of the SLA response to CO_2. Using *in situ* agricultural statistics, Calvet et al. (2012) and Canal et al. (2014) have shown that this approach is able to represent to a large extent the interannual variability of the straw cereal yields and of the forage dry matter production over France. However, extremely wet years (e.g. 2007 in Canal et al., 2014) can be interpreted by the model as favorable to cereal yield, while in the real world they may turn out unfavorable. This is caused by shortcomings in the representation of constraints on field operations, such as the lack of field accessibility (Trnka et al., 2015).

The Specific Leaf Area (SLA) response to a 50% increase in the atmospheric concentration of CO_2 (hereafter referred to as [CO_2]) is shown in Table 1 in order to illustrate the nitrogen dilution approach used in the model:

The ratio of future to past leaf mass-based nitrogen concentration is related to the ratio in [CO_2] as:

$$\frac{Future\ N_L}{Past\ N_L} = \left(\frac{Future\ [CO_2]}{Past\ [CO_2]}\right)^{-D} \quad (1)$$

where D is a nitrogen dilution parameter derived by Calvet et al. (2008) from the meta-analysis of Yin (2002) for various plant functional types. The past N_L values given in Table 1 correspond to a past [CO_2] value of 371 ppm. Values of D are given in Table 1 for the four vegetation types considered in this study (straw cereals, grasslands, broadleaf forests, and needleleaf forests). The SLA value is derived from N_L using leaf trait plasticity parameters e and f (Gibelin et al., 2006):

$$SLA = e \times N_L + f \quad (2)$$

2.4. Design of the simulations

The ISBA model is forced by the hourly atmospheric variables derived from the downscaling of the eleven climate simulations listed in Fig. 1. The simulations cover a 150-yr period, from 1950 to 2099 and three time periods are used in our

Table 1
Standard values of ISBA-A-gs parameters (Gibelin et al., 2008) for 4 vegetation types (straw cereals and C3 grasslands). The mesophyll conductance at a leaf temperature of 25 °C, in well-watered conditions, g_m, is in units of mm s^{-1}, g_c is the cuticular conductance, in mm s^{-1}, SWI_C is the critical extractable soil moisture content fraction, dimensionless, τ_{max} is the maximum leaf span time, in days, LAI_{min} is the minimum leaf area index, in $m^2\ m^{-2}$, N_L is the leaf nitrogen concentration in% of dry mass for an atmospheric CO_2 concentration of 371 ppm, e is the SLA (specific leaf area) sensitivity to N_L, in $m^2\ kg^{-1}\ \%^{-1}$, f is SLA at N_L = 0%, in $m^2\ kg^{-1}$. The nitrogen dilution parameter D (derived from Calvet et al., 2008) is dimensionless.

Vegetation type	g_m	g_c	SWI_C	Response to drought	τ_{max}	LAI_{min}	N_L	e	f	D	SLA response to +50% [CO_2]
Straw cereals	1	0.25	0.3	Avoiding	150	0.3	1.3	3.79	9.84	0.17	−2.2%
Grasslands	1	0.25	0.3	Tolerant	150	0.3	1.3	5.56	6.73	0.24	−4.8%
Broadleaf forests	3	0.15	0.3	Tolerant	230	0.3	2.0	4.83	2.53	0.45	−13.3%
Needleleaf forests	2	0.00	0.3	Avoiding	365	1.0	2.8	4.85	−0.24	0.19	−7.5%

analysis: P (1970–1999), NF (2020–2049), and DF (2070–2099). In addition to the downscaled climate simulations, mean annual values of [CO_2] consistent with the A1B scenario are used. For example: 311 ppm in 1950, 367 ppm in 2000, 522 ppm in 2050, and 700 ppm in 2099. The past [CO_2] value of 371 ppm used in Eq. (1) corresponds to year 2002.

The ISBA simulations are made for 191 grid-cells (Section 2.2). The simulations obtained for each of the four vegetation types and for each of the eleven climate models consist of 191 daily time series of LAI and root-zone soil moisture, covering a 150-yr period. In order to initialize the carbon pools, the same number of simulations is performed before starting the final simulations through a spin-up procedure using the 1950–1959 period (i.e. the 10 first years) repeated 15 times.

In order to evaluate the impact of the nitrogen dilution Eq. (1), an additional set of simulations is performed with $D = 0$, for four climate simulations: HADGEM2_1, IPCM4_1, CNCM33_1, and DMIEH5C_3.

2.5. Biophysical indicators

Four biophysical indicators derived from the ISBA simulations are used in this study. Three of them correspond to phenological dates (in units of days within each considered year): leaf onset, leaf senescence, date of maximum LAI. Annual dates of leaf onset and leaf senescence are retrieved from the LAI simulations, following Gibelin et al. (2006) and Szczypta et al. (2014). Leaf onset (senescence) corresponds to the date when the departure of LAI from its minimum annual value between 1 September of the previous year and the date of maximum LAI becomes higher (respectively, lower) than 40% of the amplitude of the annual cycle. It may happen that LAI values are higher than the 40% threshold before or after the date of maximum LAI. In this case, the minimum LAI is used to determine the date.

The fourth biophysical indicator, hereafter referred as drought duration, is the mean yearly cumulated duration of dry soil conditions. The latter are defined as mean Soil Wetness Index (SWI, dimensionless) lower than $SWI_C = 0.3$. The SWI can be written as:

$$SWI = (\theta - \theta_{WILT})/(\theta_{FC} - \theta_{WILT}) \tag{3}$$

where θ is the root-zone volumetric water content (in $m^3\ m^{-3}$), and the subscript "FC" and "WILT" indicate soil moisture at field capacity and at wilting point, respectively.

2.6. Statistical analysis

A statistical analysis is applied to the time series of the biophysical indicators in order to assess trends and uncertainties:

- The trend analysis aims at determining whether the impact of climate change on a given variable is significant or not. The Mann-Kendall trend test is applied to the 1970–2049 period for the near future (NF) conditions, and to the 1970–2099 period for the distant future (DF) conditions. The test null hypothesis is "no trend" and the null hypothesis is rejected if the test p-value is lower than 0.01.
- The uncertainty analysis evaluates the consistency of the impact of the various climate models. The ANOVA variance test is applied to NF vs. P anomalies and to DF vs. P anomalies. The test null hypothesis is "identical anomaly means" and the alternative hypothesis is "at least one climate model differs from the other models". The null hypothesis is rejected if the test p-value is lower than 0.05.

Trends and uncertainties are presented in Section 3.

2.7. Spatial classification method

The spatial patterns are identified through a clustering method, the k-means classification technique. This method is applied to anomalies of leaf onset and leaf senescence dates, in either NF or DF conditions, for the four vegetation types. This represents 16 configurations. Thirty anomaly values are considered at each site, corresponding to the 30 years of the NF or DF time period (Fig. 1). Each anomaly value consists of the mean across the 11 climate simulations listed in Fig. 1. A number of tests (not shown) demonstrated that four clusters per configuration are enough to represent the spatial variability of the impact of climate change. In order to facilitate the analysis of the results, only four configurations (among 16) are used, all in DF conditions: straw cereals leaf onset and leaf senescence, broadleaf forests leaf onset and leaf senescence. Common cluster grid-cells are used for straw cereals and grasslands (low vegetation), and for broadleaf and needleleaf forests (high vegetation). Hereafter, these two sets of cluster grid-cells are referred to as cluster 'LV' (for low vegetation) and cluster 'HV' (for high vegetation). The same cluster grid-cells are used for NF conditions, as preliminary tests showed that similar results are obtained.

This clustering method, combined with the Mann-Kendall and ANOVA statistical tests, permits the identification of five areas where specific leaf onset or leaf senescence anomaly attributes are simulated. Fig. 3 presents the correspondence between the areas and the clusters. The analysis of the results focusses on these areas and on clusters presenting the lowest uncertainty range in DF conditions.

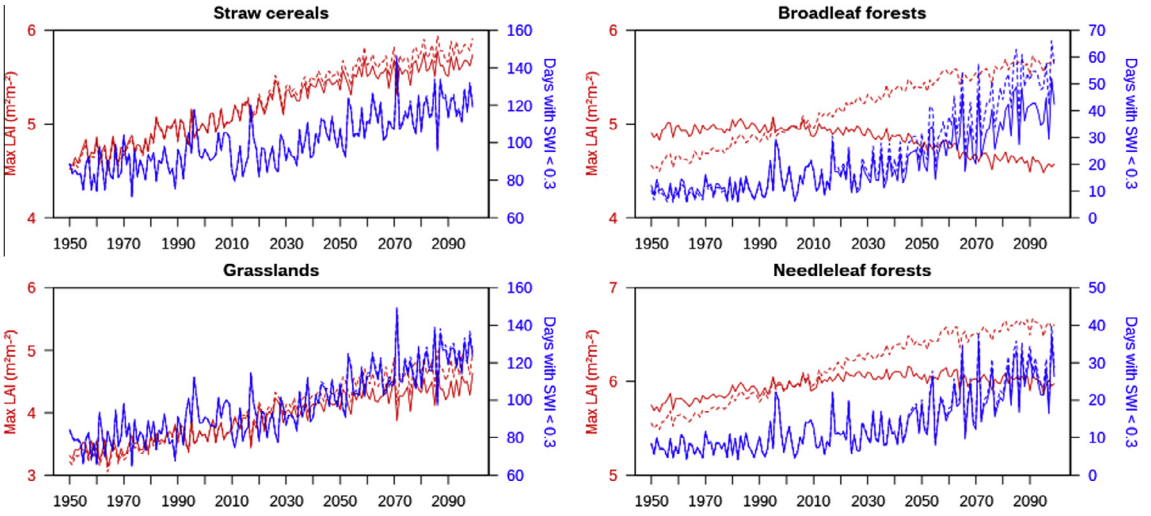

Fig. 2. Impact of climate change on (red) mean annual maximum LAI, (blue) drought duration defined as days with SWI < 0.3: (left, from top to bottom) straw cereals and grasslands, (right, from top to bottom) broadleaf and needleleaf forests, with and without nitrogen dilution in response to [CO_2] increase (solid and dashed lines, respectively). LAI and drought duration are mean values across 191 locations and four climate simulations (HADGEM2_1, IPCM4_1, CNCM33_1, DMIEH5C_3). (For interpretation of the references to color in this figure legend, the reader is referred to the web version of this article.)

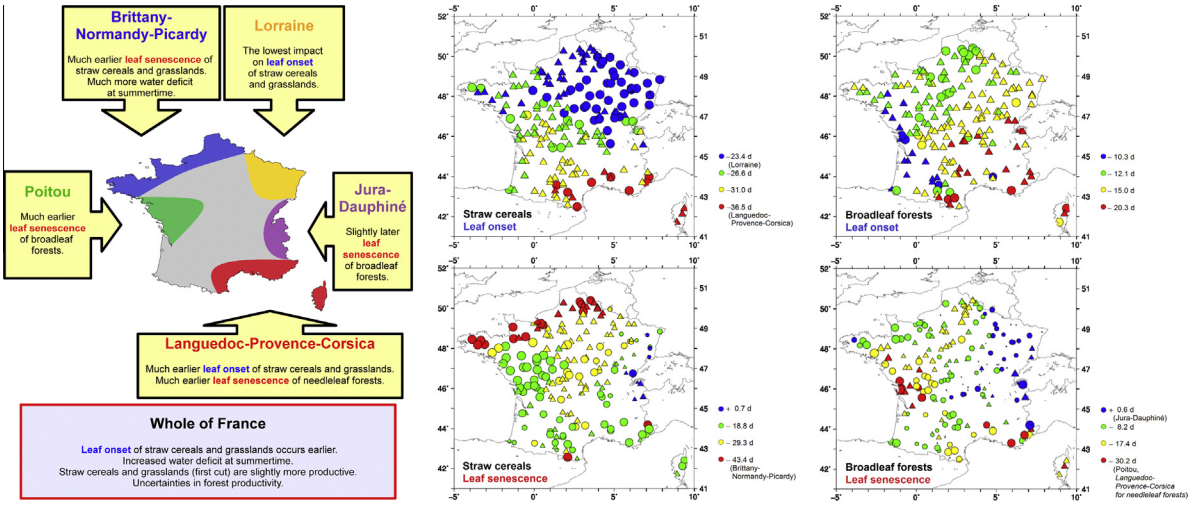

Fig. 3. Main trends in France on the phenology and on the biomass production simulated by the ISBA model related to climate change in the 21st century. (Left) overview of results. (Right) detailed regional impact of climate change at 191 locations for distant future (2070–2099) on straw cereals and broadleaf forests: (top) leaf onset anomalies, (bottom) leaf senescence anomalies (in days). The size of the symbols is proportional to the number of climatic simulations (11 as a maximum) presenting a significant trend (Mann-Kendall test). Circles denote consistent trends, triangles denote divergent trends (ANOVA test). Colors differentiate clusters: the blue, green, yellow, and red colors of the symbols are for the lowest (blue) to the highest (red) impact, i.e. cluster 1 and cluster 4, respectively. (For interpretation of the references to color in this figure legend, the reader is referred to the web version of this article.)

3. Results

3.1. Mean trends of air temperature

In order to illustrate the local climate attributes derived from the spatial downscaling of the climate simulations, Fig. 1 shows the average annual number of days with at least one hourly air temperature (T_{air}) value below freezing level (freezing days), and above 25 °C (summertime days), respectively, together with the NF and DF anomalies, at 191 locations (see Section 2.2). While the number of freezing days tends to decrease, the number of summertime days tends to increase. Fig. 1 shows that in past conditions, the average number of freezing days is larger than 100 d in the Jura-Dauphiné area, about 80 d or more in Lorraine, and lower than 40 d in Langedoc-Provence-Corsica and Poitou (see geographical information

in Fig. 3). In the latter two areas (Langedoc-Provence-Corsica and Poitou), the future anomalies in units of days are less pronounced. However, expressing the anomalies as a fraction of the past values, these areas present the largest impact of climate change on freezing days: from −20% to −50% in NF conditions, and −60% to −100% in DF conditions, to be compared with −15% to −20% in NF conditions, and −40% to −50% in DF conditions in the Lorraine and Jura-Dauphiné areas.

As far as summertime days are concerned, they are less frequent in the Brittany-Normandy-Picardy area (less than 20 d in P conditions), and more frequent in the Langedoc-Provence-Corsica area (more than 60 d in P conditions). For the Brittany-Normandy-Picardy area, their number increases less than in other regions: less than 12 d in NF conditions, less than 36 d in DF conditions. However, as for freezing days, the relative change in summertime days is more pronounced in areas presenting small numbers, such as Brittany-Normandy-Picardy: more than +50% in NF, and more than +150% in DF conditions for the area.

3.2. Mean trends of peak LAI and drought duration

The ISBA model is able to account for the antitranspirant and fertilizing effects of CO_2. In particular, the decrease in SLA related to nitrogen dilution (Section 2.3) tends to limit the increase in LAI caused by the fertilizing effect of CO_2 as shown by Fig. 2 for low vegetation (straw cereals and grasslands) and for high vegetation (broadleaf and needleleaf forests). This figure show time series of the average maximum LAI for the 150-yr period considered in this study, with and without activating the nitrogen dilution (Eq. (1)) process in the model. The same maximum LAI value is obtained in 2002, with and without activating the nitrogen dilution, as the past [CO_2] value of 371 ppm used in Eq. (1) corresponds to year 2002 (Section 2.4). After 2002, the impact of nitrogen dilution is noticeable (LAI difference higher than 0.2 $m^2\ m^{-2}$) after 2020 for broadleaf forests, 2030 for needleleaf forests, 2040 for grasslands, and 2060 for straw cereals. The impact of nitrogen dilution is more pronounced for the forests, especially for broadleaf forests. While the maximum LAI of low vegetation tends to increase, the trend observed for forests is much lower is relation to the more pronounced nitrogen dilution. In nitrogen dilution simulations, maximum LAI of broadleaf forests even tends to decrease after 2010, and after 2050 for needleleaf forests.

Fig. 2 also shows the mean drought duration, with and without activating the nitrogen dilution option. The lower LAI values obtained with the activation of nitrogen dilution generate less plant transpiration and limit the increase in drought duration. While the impact of maximum LAI on droughts is limited for low vegetation and for needleleaf forests, it is quite marked for broadleaf forests. In all cases, drought duration markedly increases after 2020.

The simulated impact of climate change and CO_2 effects on photosynthesis (or Gross Primary Production, GPP), Net Primary Production (the difference between GPP and autotrophic respiration), and the ratio of autotrophic respiration to GPP (R/GPP) is presented in the Supplement. These three quantities increase through time, especially after 2010. However, in response to the sharp increase in the R/GPP ratio, NPP tends to stabilize after 2060. The impact of nitrogen dilution on these trends is only noticeable for trees.

3.3. Trend and uncertainty mapping

The results of the statistical analysis and of the spatial classification are shown in Fig. 3 for straw cereals and for broadleaf forests in DF conditions, for both leaf onset and leaf senescence. In these maps, the size of the symbols is proportional to the number of climate models for which a significant trend in the considered biophysical variable is found. When at least one climate model differs from the other models circles are replaced by triangles. The four sorted clusters can be distinguished using colors: from blue for the lowest impact (cluster LV-1 or HV-1) to red for the largest impact (cluster LV-4 or HV-4).

For straw cereals, the leaf onset cluster LV-4 covers the Languedoc-Provence-Corsica area, and occurs 36 days earlier than in past conditions, on average. The LV-1 cluster covers the Lorraine area with a leaf onset occurring 23 days earlier than in past conditions. The leaf senescence cluster LV-4 covers the Brittany-Normandy-Picardy area and occurs 43 days earlier than in past conditions. Similar results are found for grasslands (not shown).

For high vegetation, the trends are less marked than for low vegetation and leaf onset and leaf senescence uncertainties are both more pronounced (more triangles and smaller symbols, respectively). Also, the spatial distribution of the clusters is more complex than for low vegetation.

The results of the statistical trend and uncertainty tests for leaf onset and leaf senescence are listed in the Supplement (Tables S1, S2) for the four clusters. The fraction of significant trends throughout sites and climate models (Mann-Kendall test) and the fraction of sites for which at least one climate model differs from the other models (ANOVA test) are used as metrics to characterize trends and uncertainties, respectively. The following interpretations can be proposed:

- Maximum LAI in DF conditions: for all the clusters, resulting from either leaf onset or leaf senescence classifications, the largest impact and the smallest uncertainties are observed for grasslands; the largest uncertainties are observed for broadleaf forests, which present a systematic decrease in peak LAI, while the other plant types present an increase in peak LAI. This is consistent with Fig. 2.
- Maximum LAI in NF conditions: needleleaf forests present the largest uncertainties, in relation to the relatively small response of peak LAI (Fig. 2).
- Leaf onset of straw cereals systematically displays the largest impact but uncertainty is larger than for grasslands in both DF and NF conditions.

- Leaf onset of forests presents the highest uncertainty values; the trend towards earlier leaf onset is more pronounced for needleleaf forests than for broadleaf forests in both DF and NF conditions.
- Leaf senescence presents smaller trends than leaf onset in both DF and NF conditions; needleleaf forests display the lowest uncertainty values; grasslands are often more impacted than other vegetation types; a good level of confidence is obtained for the leaf senescence cluster HV-4 that covers the Languedoc-Provence-Corsica (especially needleleaf forests in this area) and Poitou (especially broadleaf forests in this area) and cluster HV-1 over the Jura-Dauphiné area (Fig. 3); the cluster HV-4 leaf senescence occurs −30 days and −22 days earlier for broadleaf and needleleaf forests, respectively; in contrast to other areas, the cluster HV-1 leaf senescence occurs +0.6 day latter for broadleaf forests in Jura-Dauphiné.

3.4. Impact of climate change on the vegetation cycle

Fig. 4 illustrates the main findings from the trend analysis (Section 3.3), for straw cereals and broadleaf forests. The average annual cycle of LAI is shown across three 30-yr periods (P, NF, DF), for straw cereals and broadleaf forests. Each subfigure presents four clusters: leaf onset cluster 1 and cluster 4, and leaf senescence cluster 1 and cluster 4. The earlier leaf onset and the increase in peak LAI values triggered by climate change are particularly evident for straw cereals. Slightly later leaf senescence dates are observed for leaf senescence cluster LV-1 LAI cycles. Apart from these clusters, the future LAI presents lower values than past LAI at summertime (July–August) for straw cereals. For broadleaf forests, a decrease in LAI is observed during the Autumn (September–October). While leaf senescence cluster LV-1 presents systematically higher LAI values in the future, the reverse is observed for leaf senescence cluster HV-1 in September–October. Results for grasslands and needleleaf forests are presented in the Supplement.

4. Discussion

4.1. To what extent is plant phenology driven by soil moisture?

This is a key question as today *in situ* networks measuring soil moisture are much less developed than weather station networks measuring T_{air}. The drought duration indicator derived from our simulations can be used to assess the past and future impact of soil moisture on phenology. Fig. 5 presents leaf onset and leaf senescence responses of straw cereals and broadleaf forests to the mean annual T_{air} and to the annual drought duration. It appears that leaf senescence correlates better with drought duration ($r^2 > 0.9$) than with T_{air} ($r^2 < 0.8$). On the other hand, leaf onset correlates better with T_{air} than with drought duration. For grasslands and for winter crops such as straw cereals, leaf onset occurs at the beginning of spring in conditions where soil moisture content is generally close to field capacity. Leaf senescence generally occurs in dry conditions where soil moisture is the main limiting factor of plant growth. This is a consistent result, as leaf senescence occurring in dry soil conditions is the normal plant development process of cereals and grasslands.

Therefore, drought duration is a key variable to monitor the impacts of climate change on vegetation, especially in the leaf senescence cluster 4 areas in Fig. 3: Languedoc-Provence-Corsica, Brittany-Normandy-Picardy, and Poitou. This shows that developing *in situ* soil moisture networks in these areas could help monitoring the long-term impacts of climate change.

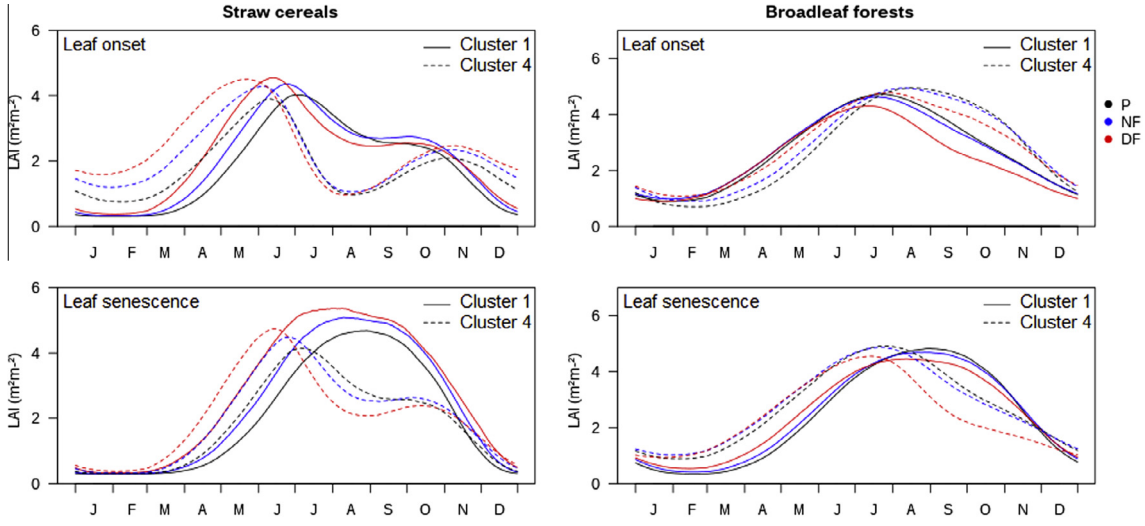

Fig. 4. Mean seasonal time series of (left) "straw cereals" and (right) "broadleaf forests" vegetation type LAI across climate models and sites within clusters presenting the (solid lines) lowest and (dashed lines) highest anomalies of (top) leaf onset and (bottom) leaf senescence, for past, near future and distant future ("P", "NF", "DF", respectively).

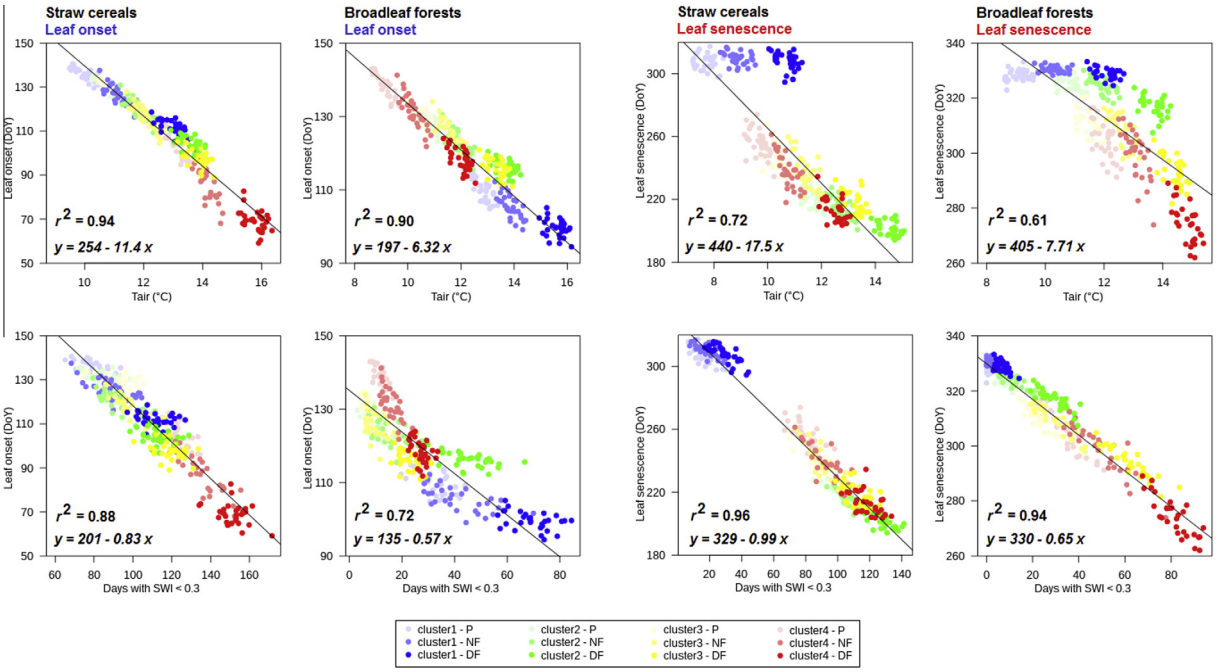

Fig. 5. Phenology indicators (in days within each considered year, or Day of Year (DoY)) vs. climatic indicators: (top) the annual mean of hourly air temperature (T_{air}) and (bottom) the mean cumulated duration of droughts defined as mean SWI < 0.3, across the 11 climate models, for the three reference 30-yr periods (P, NF, or DF). From left to right: leaf onset of straw cereals, leaf senescence of straw cereals, leaf onset of broadleaf forests, leaf senescence of broadleaf forests. Each dot corresponds to one year within a reference period, for a cluster presenting the (blue) lowest or the (red) highest anomalies. (For interpretation of the references to color in this figure legend, the reader is referred to the web version of this article.)

The type of evidence for vegetation responses shown here is also available via studies using agrometeorological indicators. While indicators based on air temperature such as growing-degree-days can be used to characterize the beginning of the growing season, the length of the growing season "is defined by soil water availability (...) in low-latitude arid regions where precipitation is primary in determining vegetation and crop growth" (Feng and Hu, 2004). Fig. 5 shows that in mid-latitude regions where soil moisture-based indicators are not relevant today, such indicators may be highly relevant in the future. For example, when all the straw cereal simulations are considered together, the leaf senescence date correlates with drought duration ($r^2 = 0.96$). On the other hand a rather poor result is obtained for Cluster 1, with $r^2 = 0.22$, showing that in this region (in eastern France), drought duration is not a very good indicator of leaf senescence, even in the future, in relation to a small change in the leaf senescence date (+0.6 d in DF conditions). Since leaf onset occurs earlier, the length of the growing season increases (see the Supplement). A similar result was obtained by Harding et al. (2015) over the UK: as drought duration does not increase, "over most of the UK the growing season length increases almost two months allowing a near year-long growing season over much of Southern England".

4.2. Uncertainties related to the CO_2 effect

The effect of atmospheric CO_2 concentration on plant growth and on nitrogen dilution has a noticeable impact on our simulations, as illustrated by Fig. 2. Eq. (1) predicts a decrease of N_L in response to rising [CO_2], in relation to nitrogen dilution. As a consequence, SLA also decreases following the leaf trait relationship Eq. (2). The combination of Eqs. (1) and (2) allows the prediction of the future SLA values. Table 1 shows that given the parameter values used for D, e, f, and N_L, the SLA decreases from about 2% for straw cereals, to 13% for broadleaf forests, in response to a rise of 50% in [CO_2]. The marked decrease of maximum LAI of broadleaf forests after 2010 shown by Fig. 2 is consistent with the higher SLA sensitivity to a rise in [CO_2] reported in Table 1. Simple calculations using Eqs. (1) and (2) show that the SLA sensitivity to [CO_2] does not vary much in response to changes in N_L. The larger sensitivity obtained for broadleaf forests is triggered by the larger value of the D nitrogen dilution parameter ($D = 0.45$) derived from the meta-analysis of Yin (2002) for this vegetation type. Following Calvet et al. (2008), we use constant values of D. However, it must be noted that Yin (2002) showed that D could be influenced to some extent by air temperature and by the incoming solar radiation. Also, studies reporting observations of the plant response to CO_2 are not always consistent (Leakey et al., 2009). For example, Gutiérrez et al. (2009) found an increase in SLA for wheat in response to [CO_2] enrichment, instead of the decrease in SLA reported by other studies. Further research is needed to progress in the simulation of the plant response to [CO_2].

Table 2
Simulated response of straw cereals to climate change (this study) vs. soft wheat CERES simulations in Brisson and Levrault (2010).

	Production increase		Leaf onset date change		Change in growing season length		ACV (*)	Change in ACV (*)	
Period	NF	DF	NF	DF	NF	DF	P	NF	DF
Brisson and Levrault (2010) (soft wheat)	+13%	+14% (Yield, France average)	−9 d	−17 d (Flowering at Mons)	−10 d	−20 d (At Mons)	0.330	−36% (Yield, at Mons)	−19%
This study (straw cereals)	+17%	+29% (Above-ground biomass, average)	−9.5 d	−23 d (Leaf onset cluster 1 mean)	−7 d	−22 d (Leaf onset cluster 1 mean)	0.065	−4% (Maximum above-ground biomass, Leaf onset cluster 1 mean)	−20%

* Annual Coefficient of Variation (ACV, i.e. ratio of the standard deviation to the mean).

4.3. Advantages and limitations of a generic approach

The generic ISBA model is neither a crop model nor a forestry model. The generic modeling approach allows the representation of the main vegetation types across the globe at various scales (from the local scale to the global scale). The differences in the simulated response of vegetation and soil variables can be easily analyzed. A limitation of this approach is that agricultural practices and forest management cannot be represented in detail. Adaptation strategies such as crop type swapping or under-planting of more suitable tree species in forests are not represented. From this point of view, our simulations provide biophysical indicators that can be used to identify climate-driven risks at given locations. But they cannot be used to provide detailed recommendations to help farmers or foresters adapt their practices. In order to fulfill this objective, specialized crop and forestry models must be used (Brisson and Levrault, 2010).

However, it must be noticed that the results summarized in Fig. 3 are consistent with the findings of Brisson and Levrault (2010) for wheat, as shown by Table 2. Quantitative information on the response of soft wheat as simulated by the CERES agricultural model (Gabrielle et al., 2002) forced by the ARPEGE A1B simulation can be found in Brisson and Levrault (2010). In particular, changes in phenological dates (wheat flowering date in particular) and in the annual coefficient of variation of yield are reported for the Mons site located in an area in northern France corresponding to the leaf onset cluster 1. For wheat, flowering occurs before maximum LAI is reached (Song et al., 2014), and changes in leaf onset dates as defined in this study can be considered as an approximation of changes in the flowering date. As shown by Table 2, changes in phenological dates are similar. Overall, trends in production increase and towards a decrease of the interannual variability are consistent. However, our large scale simulations tend to generate a lower interannual variability of the biomass production (i.e. a smaller annual coefficient of variation (ACV)) and a larger increase of the biomass production in the future. ACV values smaller than 0.1 are typical of large scale straw cereal yield statistics in France (Canal et al., 2014). Our results do not show an increase in adverse weather events able to reduce wheat yield. As shown in Table 2, our simulations indicate a reduction in the interannual variability of the maximum above-ground biomass of straw cereals: −20% in DF conditions for cluster 1. Table 2 also shows that this result is consistent with Brisson and Levrault (2010). We find a similar result for the whole of France (−16%). A different result was reported by Trnka et al. (2015), with a trend towards a larger frequency of events detrimental to wheat yield under both RCP4.5 and RCP8.5 scenarios. Over northern and western France, they found that the main cause of this trend was a decrease in field accessibility during key field operations. This difference can be explained by the fact that we do not simulate field accessibility.

Regarding forests, we checked that our simulations of Gross Primary Production (GPP) and Net Primary Production (NPP) (see the Supplement) are consistent with time series produced by the CASTANEA model in Loustau et al. (2005) for beech and oak. However, more quantitative comparisons are difficult since Loustau et al. (2005) used the B2 emissions scenario.

Another limitation of this study is the definition of the contour of specific areas with the clustering method. The spatial determination of these areas could be improved by using more grid-cells.

5. Conclusions

In spite of the increased water deficit at summertime in France, winter straw cereals and grasslands (first cut) should be slightly more productive at the end of the century than today, in relation to earlier leaf onset dates, with greatest changes in leaf onset occurring in Languedoc-Provence-Corsica. Brittany-Normandy-Picardy would experience a much more pronounced soil water deficit at summertime, resulting in much earlier leaf senescence and shorter growing season length of straw cereals and grasslands. On the other hand, we might expect smaller changes in Lorraine. Future forest productivity as a whole is affected by large uncertainties. However, it seems likely that leaf senescence will occur much earlier in Poitou for broadleaf forests, and slightly later in Jura-Dauphiné. Leaf senescence should occur much earlier in Languedoc-Provence-Corsica for needleleaf forests.

Although we used a generic approach unable to simulate agricultural and forestry practices, our results are consistent with the findings of Brisson and Levrault (2010), who used specialized crop and forestry models. With respect to previous

studies, we performed a more extensive spatial analysis of the impact of climate change, at 191 locations. Trends were analyzed in NF and DF conditions, together with the consistency of the biophysical variables across climate simulations. We analyzed the uncertainties related to climate simulations. The largest uncertainties on peak LAI values are observed for needleleaf forests in NF conditions and for broadleaf forests in DF conditions. Forests also present the largest uncertainties for leaf onset. Although leaf onset of straw cereals is more impacted than for grasslands, uncertainties are larger.

Using the plant trait meta-analysis of Yin (2002), we investigated the impact of CO_2 on plant morphology and we found a larger sensitivity for broadleaf forests triggered by a larger nitrogen dilution. Further research is needed to progress in the simulation of the plant response to [CO_2] as this is a key process.

Since the SURFEX modeling platform is able to work at a global scale, the approach used in this study could be applied to other regions in future works provided downscaled climate simulations are available. In particular, new CMIP5 RCP climate simulations could be used.

Acknowledgements

This work was supported by ANR in the framework of the ORACLE project (ANR-10-CEPL-011). We thank Nathalie de Noblet (LSCE) and Iñaki Garcia de Cortazar Atauri (INRA) for their helpful comments and advices, and Catherine Meurey (CNRM) for technical support. We want to pay tribute to the memory of Nadine Brisson (INRA), who played a key role in the initiation of this project.

Appendix A. Supplementary data

Supplementary data associated with this article can be found, in the online version, at http://dx.doi.org/10.1016/j.crm.2016.06.001.

References

Balzarolo, M., Boussetta, S., Balsamo, G., Beljaars, A., Maignan, F., Calvet, J.-C., Lafont, S., Barbu, A., Poulter, B., Chevallier, F., Szczypta, C., Papale, D., 2014. Evaluating the potential of large scale simulations to predict carbon fluxes of terrestrial ecosystems over a European Eddy Covariance network. Biogeosciences 11, 2661–2678. http://dx.doi.org/10.5194/bg-11-2661-2014.

Boé, J., Terray, L., 2008. A weather-type approach to analyzing winter precipitation in France: twentieth-century trends and the role of anthropogenic forcing. J. Clim. 21, 3118–3133. http://dx.doi.org/10.1175/2007JCLI1796.1.

Boé, J., Terray, L., Habets, F., Martin, E., 2006. A simple statistical-dynamical downscaling scheme based on weather types and conditional resampling. J. Geophys. Res. 111, D23106. http://dx.doi.org/10.1029/2005JD006889.

Boone, A., Calvet, J.-C., Noilhan, J., 1999. Inclusion of a third soil layer in a land-surface scheme using the force-restore method. J. Appl. Meteorol. 38 (11), 1611–1630.

Brisson, N., Levrault, F. (Eds.), 2010. Livre vert du projet Climator, Changement climatique, agriculture et forêt en France: simulations d'impacts sur les principales espèces. ANR, INRA, ADEME, ADEME éditions, 334 pp.

Calvet, J.-C., 2000. Investigating soil and atmospheric plant water stress using physiological and micrometeorological data sets. Agric. For. Meteorol. 103 (3), 229–247.

Calvet, J.-C., Soussana, J.-F., 2001. Modelling CO_2-enrichment effects using an interactive vegetation SVAT scheme. Agric. For. Meteorol. 108 (2), 129–152.

Calvet, J.-C., Rivalland, V., Picon-Cochard, C., Guehl, J.-M., 2004. Modelling forest transpiration and CO_2 fluxes – response to soil moisture stress. Agric. For. Meteorol. 124 (3–4), 143–156. http://dx.doi.org/10.1016/j.agrformet.2004.01.007.

Calvet, J.-C., Fritz, N., Froissard, F., Suquia, D., Petitpa, A., Piguet, B., 2007. In situ soil moisture observations for the CAL/VAL of SMOS: the SMOSMANIA network. In: Proceedings of the International Geoscience and Remote Sensing Symposium, IGARSS, Barcelona. http://dx.doi.org/10.1109/IGARSS.2007.4423019.

Calvet, J.-C., Gibelin, A.-L., Roujean, J.-L., Martin, E., Le Moigne, P., Douville, H., Noilhan, J., 2008. Past and future scenarios of the effect of carbon dioxide on plant growth and transpiration for three vegetation types of southwestern France. Atmos. Chem. Phys. 8, 397–406. http://dx.doi.org/10.5194/acp-8-397-2008.

Calvet, J.-C., Lafont, S., Cloppet, E., Souverain, F., Badeau, V., Le Bas, C., 2012. Use of agricultural statistics to verify the interannual variability in land surface models: a case study over France with ISBA-A-gs. Geosci. Model Dev. 5, 37–54. http://dx.doi.org/10.5194/gmd-5-37-2012.

Canal, N., Calvet, J.-C., Decharme, B., Carrer, D., Lafont, S., Pigeon, G., 2014. Evaluation of root water uptake in the ISBA-A-gs land surface model using agricultural yield statistics over France. Hydrol. Earth Syst. Sci. 18, 4979–4999. http://dx.doi.org/10.5194/hess-18-4979-2014.

Carrer, D., Lafont, S., Roujean, J.-L., Calvet, J.-C., Meurey, C., Le Moigne, P., Trigo, I., 2012. Incoming solar and infrared radiation derived from METEOSAT: impact on the modelled land water and energy budget over France. J. Hydrometeorol. 13, 504–520. http://dx.doi.org/10.1175/JHM-D-11-059.1.

Carrer, D., Roujean, J.-L., Lafont, S., Calvet, J.-C., Boone, A., Decharme, B., Delire, C., Gastellu-Etchegorry, J.-P., 2013. A canopy radiative transfer scheme with explicit FAPAR for the interactive vegetation model ISBA-A-gs: impact on carbon fluxes. J. Geophys. Res. Biogeosci. 118, 888–903. http://dx.doi.org/10.1002/jgrg.20070.

Déqué, M., Somot, S., 2010. Weighted frequency distributions expressing modelling uncertainties in the ENSEMBLES regional climate experiments. Clim. Res. 44 (2–3), 195–209. http://dx.doi.org/10.3354/cr00866.

Durand, Y., Brun, E., Merindol, L., Guyomarc'h, G., Lesaffre, B., Martin, E., 1993. A meteorological estimation of relevant parameters for snow models. Ann. Glaciol. 18, 65–71.

Feng, S., Hu, Q., 2004. Changes in agro-meteorological indicators in the contiguous United States: 1951–2000. Theor. Appl. Climatol. 78, 247–264. http://dx.doi.org/10.1007/s00704-004-0061-8.

Gabrielle, B., Roche, R., Angas, P., Cantero-Martinez, C., Cosentino, L., Mantineo, M., Langensiepen, M., Hénault, C., Laville, P., Nicoullaud, B., Gosse, G., 2002. A priori parametrisation of the CERES soil-crop models and tests against several European data sets. Agronomie 22, 25–38. http://dx.doi.org/10.1051/agro:2002003.

Garrigues, S., Olioso, A., Calvet, J.-C., Martin, E., Lafont, S., Moulin, S., Chanzy, A., Marloie, O., Buis, S., Desfonds, V., Bertrand, N., Renard, D., 2015. Evaluation of land surface model simulations of evapotranspiration over a 12-year crop succession: impact of soil hydraulic and vegetation properties. Hydrol. Earth Syst. Sci. 19, 3109–3131. http://dx.doi.org/10.5194/hess-19-3109-2015.

Gibelin, A.-L., Calvet, J.-C., Roujean, J.-L., Jarlan, L., Los, S.O., 2006. Ability of the land surface model ISBA-A-gs to simulate leaf area index at the global scale: comparison with satellites products. J. Geophys. Res. 111 (D18), D18102. http://dx.doi.org/10.1029/2005JD006691.

Gibelin, A.-L., Calvet, J.-C., Viovy, N., 2008. Modelling energy and CO_2 fluxes with an interactive vegetation land surface model – evaluation at high and middle latitudes. Agric. For. Meteorol. 148, 1611–1628.

Gouache, D., Le Bris, X., Bogard, M., Deudon, O., Pagé, C., Gate, P., 2012. Evaluating agronomic adaptation options to increasing heat stress under climate change during wheat grain filling in France. Eur. J. Agron. 39, 62–70. http://dx.doi.org/10.1016/j.eja.2012.01.009.

Gutiérrez, E., Gutiérrez, D., Morcuende, R., Verdejo, A.L., Kostadinova, S., Martinez-Carrasco, R., Pérez, P., 2009. Changes in leaf morphology and compositions with future increases in CO_2 and temperature revisited: wheat in field chambers. J. Plant Growth Regul. 28, 349–357. http://dx.doi.org/10.1007/s00344-009-9102-y.

Habets, F., Boé, J., Déqué, M., Ducharne, A., Gascoin, S., Hachour, A., Martin, E., Pagé, C., Sauquet, E., Terray, L., Thiéry, D., Oudin, L., Viennot, P., 2013. Impact of climate change on the hydrogeology of two basins in northern France. Clim. Change 121 (4), 771–785. http://dx.doi.org/10.1007/s10584-013-0934-x.

Harding, A.E., Rivington, M., Mineter, M.J., Tett, S.F.B., 2015. Agro-meteorological indices and climate model uncertainty over the UK. Clim. Change 128, 113–126. http://dx.doi.org/10.1007/s10584-014-1296-8.

IFN, 2011. Inventaire forestier national, une nouvelle partition écologique et forestière du territoire métropolitain: les sylvoécorégions. L'IF. 26, 8 pp. Available on: <http://inventaire-forestier.ign.fr/spip/IMG/pdf/IF_SER_web.pdf>.

IPCC SRES, 2000. In: Nakićenović, N., Swart, R. (Eds.), Special Report on Emissions Scenarios: A Special Report of Working Group III of the Intergovernmental Panel on Climate Change. Cambridge University Press, UK.

Jacob, D., Petersen, J., Eggert, B., Alias, A., Christensen, O.B., Bouwer, L.M., Braun, A., Colette, A., Déqué, M., Georgievski, G., Georgopoulou, E., Gobiet, A., Laurent Menut, L., Nikulin, G., Haensler, A., Hempelmann, N., Jones, C., Keuler, K., Kovats, S., Kröner, N., Kotlarski, S., Kriegsmann, A., Martin, E., van Meijgaard, E., Moseley, C., Pfeifer, S., Preuschmann, S., Radermacher, C., Radtke, K., Rechid, D., Rounsevell, M., Samuelsson, P., Somot, S., Soussana, J.-F., Teichmann, C., Valentini, R., Vautard, R., Weber, B., Yiou, P., 2014. EURO-CORDEX: new high-resolution climate change projections for European impact research. Reg. Environ. Change 14, 563–578. http://dx.doi.org/10.1007/s10113-013-0499-2.

Lafont, S., Zhao, Y., Calvet, J.-C., Peylin, P., Ciais, P., Maignan, F., Weiss, M., 2012. Modelling LAI, surface water and carbon fluxes at high-resolution over France: comparison of ISBA-A-gs and ORCHIDEE. Biogeosciences 9, 439–456. http://dx.doi.org/10.5194/bg-9-439-2012.

Leakey, A.D.B., Ainsworth, E.A., Bernacchi, C.J., Rogers, A., Long, S.P., Ort, D.R., 2009. Elevated CO_2 effects on plant carbon, nitrogen, and water relations: six important lessons from FACE. J. Exp. Bot. 60, 2859–2876. http://dx.doi.org/10.1093/jxb/erp096.

Loustau, D., Bosc, A., Colin, A., Ogée, J., Davi, H., François, C., Dufrêne, E., Déqué, M., Cloppet, E., Arrouays, D., Le Bas, C., Saby, N., Pignard, G., Hamza, N., Granier, A., Bréda, N., Ciais, P., Viovy, N., Delage, F., 2005. Modeling climate change effects on the potential production of French plains forests at the sub-regional level. Tree Physiol. 25, 813–823.

Masson, V., Le Moigne, P., Martin, E., Faroux, S., Alias, A., Alkama, R., Belamari, S., Barbu, A., Boone, A., Bouyssel, F., Brousseau, P., Brun, E., Calvet, J.-C., Carrer, D., Decharme, B., Delire, C., Donier, S., Essaouini, K., Gibelin, A.-L., Giordani, H., Habets, F., Jidane, M., Kerdraon, G., Kourzeneva, E., Lafaysse, M., Lafont, S., Lebeaupin Brossier, C., Lemonsu, A., Mahfouf, J.-F., Marguinaud, P., Mokhtari, M., Morin, S., Pigeon, G., Salgado, R., Seity, Y., Taillefer, F., Tanguy, G., Tulet, P., Vincendon, B., Vionnet, V., Voldoire, A., 2013. The SURFEX v7.2 land and ocean surface platform for coupled or offline simulation of Earth surface variables and fluxes. Geosci. Model Dev. 6, 929–960. http://dx.doi.org/10.5194/gmd-6-929-2013.

Pagé, C., Terray, L., 2010. Nouvelles projections climatiques à échelle fine sur la France pour le 21ème siècle: les scénarii SCRATCH2010. Technical Report TR/CMGC/10/58. Centre Européen de Recherche et de Formation Avancée en Calcul Scientifique (CERFACS), Toulouse, France. Available at: <~page/publications/report_cerfacs_regional_scenarii_scratch2010.pdf" xlink:type="simple" id="ir020">http://www.cerfacs.fr/~page/publications/report_cerfacs_regional_scenarii_scratch2010.pdf>.

Pagé, C., Terray, L., Boé, J., 2010. dsclim: A Software Package to Downscale Climate Scenarios at Regional Scale Using a Weather-Typing Based Statistical Methodology. Technical Report TR/CMGC/09/21. Centre Européen de Recherche et de Formation Avancée en Calcul Scientifique (CERFACS), Toulouse, France. Available at: <~page/dsclim/dsclim_doc-latest.pdf" xlink:type="simple" id="ir025">http://www.cerfacs.fr/~page/dsclim/dsclim_doc-latest.pdf>.

Quintana-Segui, P., Lemoigne, P., Durand, Y., Martin, E., Habets, F., Baillon, M., Canellas, C., Franchisteguy, L., Morel, S., 2008. Analysis of near surface atmospheric variables: validation of the SAFRAN analysis over France. J. Appl. Meteorol. Clim. 47, 92–107.

Song, X., Cui, B., Yang, G., Feng, H., 2014. Comparison of winter wheat growth with multi-temporal remote sensing imagery. 35th International Symposium on Remote Sensing of Environment. IOP Conf. Series: Earth and Environmental Science, vol. 17. http://dx.doi.org/10.1088/1755-1315/17/1/012044.

Soussana, J.-F., Graux, A.I., Tubiello, F.N., 2010. Improving the use of modelling for projections of climate change impacts on crops and pastures. J. Exp. Bot. 61, 2217–2228. http://dx.doi.org/10.1093/jxb/erq100.

Szczypta, C., Calvet, J.-C., Maignan, F., Dorigo, W., Baret, F., Ciais, P., 2014. Suitability of modelled and remotely sensed essential climate variables for monitoring Euro-Mediterranean droughts. Geosci. Model Dev. 7, 931–946. http://dx.doi.org/10.5194/gmd-7-931-2014.

Trnka, M., Hlavinka, P., Semenov, M.A., 2015. Adaptation options for wheat in Europe will be limited by increased adverse weather events under climate change. J. R. Soc. Interface 12, 20150721. http://dx.doi.org/10.1098/rsif.2015.0721.

Tubiello, F.N., Soussana, J.-F., Howden, S.M., Easterling, W., 2007. Crop and pasture response to climate change. Proc. Natl. Acad. Sci. U.S.A. 104, 19686–19690. http://dx.doi.org/10.1073/pnas.0701728104.

Yin, X., 2002. Responses of leaf nitrogen concentration and specific leaf area to atmospheric CO_2 enrichment: a retrospective synthesis across 62 species. Glob. Change Biol. 8 (7), 631–642.